J Mater Sci (2018) 53:15237–15245

Electronic materials

Structural and electrical properties of Ge-doped ZrO_2 thin films grown by atomic layer deposition for high-k dielectrics

Bo-Eun Park[1], Yujin Lee[1], Il-Kwon Oh[1], Wontae Noh[2], Satoko Gatineau[2], and Hyungjun Kim[1,*]

[1] School of Electrical and Electronic Engineering, Yonsei University, 50 Yonsei-ro, Seodaemun-gu, Seoul 03722, Korea
[2] Air Liquide Korea Co, Yonsei University, 50 Yonsei-ro, Seodaemun-gu, Seoul 03722, Korea

Received: 21 January 2018
Accepted: 10 July 2018
Published online: 6 August 2018

ABSTRACT

Enhancing the dielectric constant (k) of conventional gate dielectric materials such as HfO_2 and ZrO_2 is one of the important requirements for further scaling down of devices in future years. One promising approach for achieving this is to incorporate a specific element in the high-k host material for stabilizing a particular higher-k crystalline phase. Although Ge has been theoretically suggested as a stabilizer for ZrO_2, there are no experimental studies correlating the structure of ZrO_2 films fabricated by atomic layer deposition (ALD) with their electrical properties. In this work, we systematically investigated the structural and electrical properties of Ge-doped ZrO_2 films prepared by ALD. We used germanium butoxide ($Ge(O^nBu)_4$) and Zr tris(dimethylamino)cyclopentadienyl zirconium as the Ge and Zr precursors, respectively, with O_3 as a reactant. We controlled the ALD cycle ratio using a supercycle process (GeO_2/ZrO_2 = 1:128, 1:64, 1:32, 1:16, 1:8, 1:4, and 1:2) to produce the alloy films. Electrical properties of these samples were evaluated by measuring the electrical characteristics of metal-oxide-semiconductor (MOS) capacitors based on them, and the results are discussed together with crystallographic analysis. The results revealed that Ge incorporation into ZrO_2 induced the stabilization of the cubic/tetragonal phase of the ZrO_2 film at low temperatures and improved its dielectric properties. Consequently, this is a systematic and facile method to optimize the dielectric properties of Ge-doped ZrO_2 prepared by varying the ALD cycle ratio, and these films could be applied in future nanoscale devices.

Bo-Eun Park, Yujin Lee, and Il-Kwon Oh contributed equally to this work.

Address correspondence to E-mail: hyungjun@yonsei.ac.kr

https://doi.org/10.1007/s10853-018-2695-4

Introduction

With the continuous scaling down of metal-oxide-semiconductor field-effect transistors (MOSFETs) for logic devices and metal-insulator-metal (MIM) capacitors for memory devices, materials with a high dielectric constant (k) have been introduced. ZrO_2 is one of the most promising high-k materials investigated to date, since it has good thermal stability, dielectric properties with a high dielectric constant ($k \sim 20$), and a wide bandgap (5.16–7.8 eV) [1–3]. There are several polymorphs of ZrO_2 with different dielectric constants. It has been found theoretically that cubic and tetragonal ZrO_2 have higher k values, over 30, than those of the monoclinic ($k \sim 16$–20) and amorphous ($k \sim 16$–20) phases [4]. With increasing temperature, the phase of ZrO_2 changes from monoclinic (< 1400 K) to tetragonal (1400–2570 K) and then to cubic (2570–2980 K). Cubic and tetragonal phases of ZrO_2 are not easily formed since they are metastable at room temperature.

There have been studies on doping ZrO_2 with aliovalent elements such as Y [5–7], La [8], and Ta [9] in ZrO_2 films to stabilize the cubic/tetragonal phase of ZrO_2. Doping ZrO_2 with these elements introduces oxygen vacancies for charge compensation, leading to the stabilization of the cubic/tetragonal phase of ZrO_2 at low temperatures. For example, upon doping ZrO_2 with Y, oxygen vacancies are generated by the substitution of Y for Zr atoms, so that the crystalline structure of ZrO_2 is transformed into the cubic/tetragonal phase [5]. In another study, increasing the La content suppressed the monoclinic phase and stabilized the tetragonal or cubic phase of ZrO_2 [8]. In contrast, tetravalent elements such as Si, Ti, Ce, and Ge can also stabilize the cubic/tetragonal phase of ZrO_2 at low temperatures without introducing oxygen vacancies [10–13]. If a tetravalent dopant is substituted for Zr atoms, the ZrO_2 structure is transformed into the cubic or tetragonal phase, since the dopant–O atom distance is different than that of Zr–O atom. For example, Ce doping decreased the crystallization temperature and increased the dielectric constant of ZrO_2 without introducing oxygen vacancies [11]. Furthermore, first-principle calculations suggest that Ge and Si could be promising stabilizers for the cubic/ tetragonal phases of ZrO_2, since Ge and Si have the same valence states as the Zr atom [13].

So far, however, only a few studies have been reported on doping Ge or Si for the stabilization of ZrO_2 or HfO_2 [12, 14, 15]. For example, Tomida et al. reported that Si doping could stabilize the tetragonal phase of HfO_2 obtained by cosputtering HfO_2 and SiO_2 targets [12]. Only one research group has reported the phase stabilization of ZrO_2 due to Ge doping. Tsoutsou et al. demonstrated that the incorporation of Ge into ZrO_2 on a SiON/Si substrate using molecular beam epitaxy (MBE) resulted in the stabilization of the tetragonal phase at low Ge contents (3–6.2 at.%) and low growth temperatures (225–360 °C). Phase stabilization was proven by analysis of the tetragonality based on the unit cell parameters (c and a) of the tetragonal ZrO_2 structure. They reported that the enhancement of the dielectric constant could be attributed to the increase in the tetragonality and the obtained tetragonal ZrO_2 could be beneficial for the integration of this dielectric in scaled devices, due to its excellent thermal stability and low equivalent oxide thickness [14, 15]. However, the sputtering process cannot be used for the deposition of high-k layers in complementary metal-oxide-semiconductor (CMOS) devices due to poor conformality and ion bombardment to the region underneath the surface of the substrate. Although the MBE process is an epitaxy method for depositing high-quality thin films, its productivity is low, which leads to obvious financial burdens. Meanwhile, atomic layer deposition (ALD), based on self-limiting growth on the surface, is considered to be one of the most promising thin film deposition techniques for enabling nanoscale device fabrication (such as CMOS devices, memory devices, photovoltaic devices) owing to its ability to control atomic-scale thickness, low contamination by impurities, and excellent conformality [16–18]. The supercycle process of ALD, which involves one ALD cycle for the dopant and n repetitions of ALD cycle for the host material, enables us to dope different amounts of Ge. However, although this method allows fine control of the film contents and can produce high-quality films, the use of ALD to prepare Ge-doped ZrO_2 has not been experimentally demonstrated. Since the growth mechanism of ALD is completely different from that of other methods referred to previously, we believe that the investigation of Ge-doped ZrO_2 films prepared by ALD will have industrial impacts. With practical applications in the semiconductor field, especially for the deposition of gate dielectrics, ALD is an essential process for mass production since it can provide precise control over composition and reproducibility. Moreover, properties such as the

interface trap density (D_{it}) and leakage current density with respect to the interface quality and insulating properties, as well as the dielectric constant, should be comprehensively examined and discussed along with the microstructure and crystallinity of the films.

In this article, we investigated the properties of Ge-doped ZrO_2 films fabricated by ALD as a function of the Ge content by controlling the GeO_2/ZrO_2 cycle ratios. To the best of our knowledge, this is the first report on the evaluation of the structural and electrical properties of Ge-doped ZrO_2 films prepared by ALD. Based on the Ge content, we mainly focused on the phase stabilization of Ge-doped ZrO_2, which was studied in correlation with the crystallographic phase and grain size. In addition, the electrical properties of Ge-doped ZrO_2, such as the capacitance and leakage current density, were investigated. Thus, we systematically analyzed the effect of phase stabilization induced by the doping of ZrO_2 with Ge on its electrical properties.

Experimental details

For this study, we used a commercial ALD chamber (ALD5008 of SNTEK Co.). This setup has a double shower-head system for improved uniformity. For ALD, germanium butoxide ($Ge(O^nBu)_4$) and tris(dimethylamino)cyclopentadienyl zirconium ($(C_5H_5)Zr[N(CH_3)_2]_3$) were used as the Ge and Zr precursors, respectively. Each of these precursors was contained in a stainless-steel bubbler, which was heated to 105–40 °C, respectively, to achieve sufficient vapor pressures. Both precursor vapors were transported to a reaction chamber using Ar as the carrier gas, whose flow rate of 50 sccm was controlled by a mass flow controller (MFC). Ar gas with the same flow rate was used to purge the excess gas molecules and by-products between each precursor and reactant exposure step. O_3 was used as the reactant for O_3-based ALD, and its concentration (8%) was controlled by an ozone generator (MKS AX 8200 of Applied Materials). The process timings for the precursor exposure–purge–reactance exposure–purge sequence was 2–5–2–5 s and 2–5–1–5 s for the ALD of GeO_2 and ZrO_2, respectively. The saturated growth-per-cycle (GPC) of GeO_2 and ZrO_2 was ~ 0.3 and 0.8 Å/cycle, respectively. An ALD supercycle process was utilized to accomplish GeO_2 doping into ZrO_2. The supercycle is composed of one ALD GeO_2 cycle, followed by n repetitions of the ALD ZrO_2 cycles, as schematically and described in Figure S1. Here, the number of ZrO_2 ALD cycles per supercycle, n, was modulated between $n = 2$ and $n = 128$ ($GeO_2/ZrO_2 = 1{:}n$ with $n = 2$, 4, 8, 16, 32, 64, and 128). By using this process, we modulated the Ge/(Ge + Zr) composition of the Ge-doped ZrO_2 films. The substrate temperature was maintained at 300 °C throughout the ALD process.

The thickness and refractive index of the films were measured by spectroscopic ellipsometry (Elli-SE-F of Ellipso Technology). The chemical composition and impurity contents were analyzed by X-ray photoelectron spectroscopy (XPS, AXIS NOVA of KRATOS) with a monochromatic Al $K\alpha$ source (beam energy 1486.6 eV and analysis area 100 μm^2). Before measurement, 60-s sputtering with Ar^+ ion bombardment was performed for surface cleaning. The microstructure of the films was analyzed by X-ray diffraction (XRD, ATX-G of Rigaku).

For metal oxide semiconductor (MOS) capacitor fabrication, Ge-doped ZrO_2 films fabricated by ALD were deposited on p-type Si substrates. Then, post-deposition annealing was carried out using a rapid thermal annealing system under an N_2 environment at 400 °C for 10 min. Subsequently, Ru was deposited as a top electrode using DC magnetron sputtering with a plasma power of 30 W through a patterned shadow mask. The thickness of Ru was 100 nm, and the diameter of the patterned dot was 100 μm. Electrical properties based on capacitance–voltage (C–V) and current–voltage (I–V) characteristics of Ge-doped ZrO_2 were evaluated using a Keithley 590 C–V analyzer and Agilent 4155 C semiconductor parameter analyzer, respectively. D_{it} was determined by the conductance method using a following equation:

$$D_{it} = \left(\frac{G_p}{\omega}\right)_{max} [qf_D(\sigma_s)A]^{-1} \quad (1)$$

where Gp/ω is a corrected conductance loss, ω is the angular frequency ($\omega = 2\pi f$, f is the measurement frequency), q is the electronic charge (1.6×10^{19} °C), f_D is a universal function that depends on the standard deviation of band bending σ_s, and A is the area of the metal gate. In our previous publication, a more detailed description of the electrical evaluation can be found [19].

Results and discussion

Figure 1a, b, c shows the XPS spectra of Zr 3d, O 1 s, and Ge 2p core levels, respectively, for Ge-doped ZrO_2 obtained by varying the GeO_2/ZrO_2 cycle ratios using the ALD supercycle process. The measured Zr 3d peaks (Fig. 1a) were deconvoluted into two sub-peaks; the peaks at 184.5 and 182.0 eV are assigned to Zr $3d_{3/2}$ and Zr $3d_{5/2}$, respectively, and these peaks show the typical characteristics of ZrO_2 [20]. As the ALD cycle ratio (GeO_2/ZrO_2) increases, the peaks corresponding to the Zr content in the films gradually decreased, indicating that the ALD supercycle gradually modulates the dopant concentration in the host material. In the O 1 s core level spectra, the peaks were deconvoluted into three sub-peaks as shown in Figure S3; the peaks at ~ 530.3 eV and ~ 531.8 eV are assigned to Zr–O–Zr bonding and Zr–OH bonding [21], respectively, and the peak at ~ 532.3 eV is assigned to GeO_2 [22]. Upon increasing the ALD cycle ratio, this area gradually increased, resulting in asymmetric shapes, indicating increased GeO_2 content. The GeO_2 content is shown in Fig. 1d. Figure 1c shows the Ge peaks in Ge_2 p core level spectra. The Ge peak intensity for 1:128 and 1:64 Ge-doped ZrO_2 samples was too weak to be observed, indicating that the Ge concentrations in these films were under the resolution limit (0.1–1 at.%) of XPS. For the other samples, one main peak at 1219.5 eV is assigned to the Ge–O bond, corresponding to GeO_2. The intensity of this peak increased with increasing ALD cycle ratio, indicating an increase in the Ge content in the films. At the ALD cycle ratio of 1:8 and 1:4, the Ge metallic state is observed as a small shoulder at ~ 1217.0 eV due to Ar^+ ion bombardment before XPS analysis [23]. Other peaks from impurity elements such as nitrogen and carbon were rarely detected, indicating high purity of all the samples (Figure S2). Figure 1d shows the GeO_2 ratio obtained from O 1 s core level spectra and Ge contents, which were measured and estimated from the deconvolution of the XPS spectra in Figure S3, in the Ge-doped ZrO_2 films as a function of the ALD cycle ratio of GeO_2 to ZrO_2. The Ge content (Ge/(Ge + Zr)) was determined by XPS, and the values are summarized in Table 1. The Ge content was also estimated by considering the GPC of GeO_2 and ZrO_2, using the following formula:

$$\text{Ge content} = \frac{(\text{GPC})_{GeO_2} \times (\text{Cycle ratio})_{GeO_2}}{(\text{GPC})_{GeO_2} \times (\text{Cycle ratio})_{GeO_2} + (\text{GPC})_{ZrO_2} \times (\text{Cycle ratio})_{ZrO_2}} \quad (2)$$

The two curves in Fig. 1d, corresponding to the measured and estimated amount of Ge in Ge-doped ZrO_2 films, show similar trends, with the Ge content gradually increasing with increasing GeO_2 cycle ratio. However, the Ge contents determined by XPS are slightly lower than those estimated by GPC. This discrepancy between the expected and measured values for the supercycle process is usually observed due to differences in the molecular adsorption surface environment between pristine and doped thin films [24]. However, these XPS results indicate that the ALD supercycle process allows us to easily modulate the Ge content by controlling the GeO_2/ZrO_2 cycle ratio in the ALD.

The crystallographic phases of the Ge-doped ZrO_2 films deposited on p-type Si with varying GeO_2/ZrO_2 cycle ratios in ALD were analyzed by XRD after N_2 annealing at 400 °C (Fig. 2a). Undoped ZrO_2 films exhibited a weak peak at 30.7° corresponding to the (111) plane of cubic/tetragonal phase, in agreement with previous reports on the existence of cubic/tetragonal phases in undoped ZrO_2 grown by ALD [8, 25]. For the 1:128 Ge-doped ZrO_2 sample, the intensity of the cubic/tetragonal (111) peak significantly increased and new peaks corresponding to cubic/tetragonal (200) plane and the monoclinic (111) plane appeared at 35.6° and 31.6°, respectively. Substitution of Zr with a dopant can change the atomic arrangement of the lattice due to the different atomic radius and electronegativity of the dopant, leading to stabilization or transformation of the crystal phase. In this work, Ge incorporation into ZrO_2 stabilized the cubic/tetragonal phase, corresponding to previous reports on Ge-doped ZrO_2 [14, 15]. However, when the solubility limit of Ge in ZrO_2 is exceeded by 3–5%, Ge atoms do not substitute Zr atoms significantly;

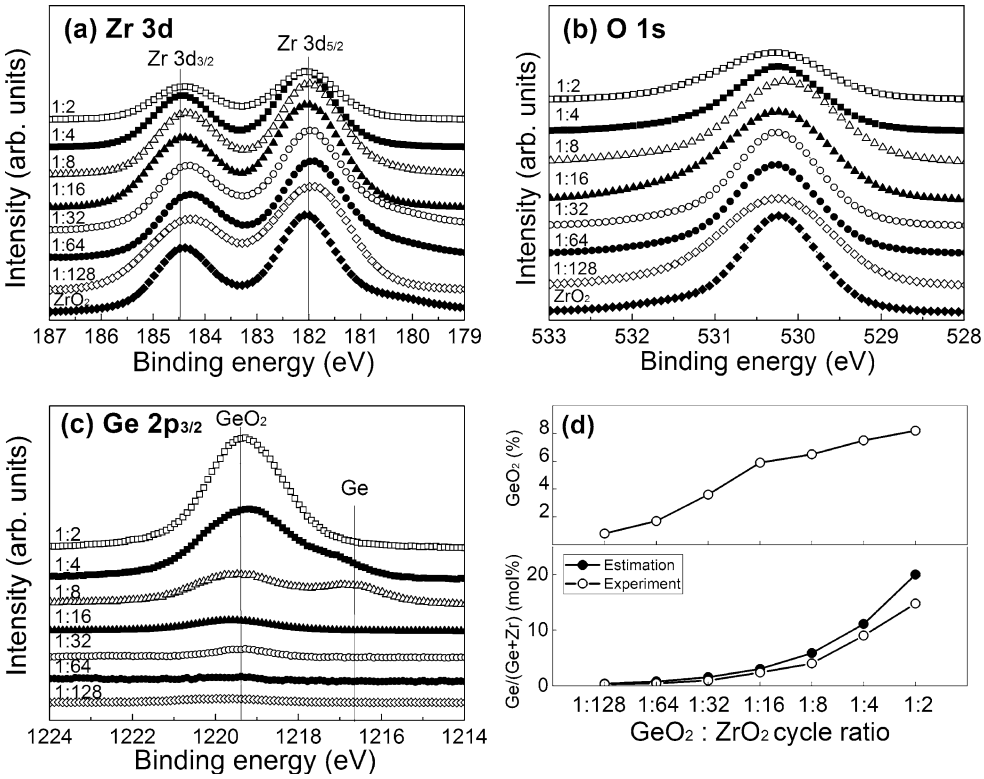

Figure 1 XPS spectra of Ge-doped ZrO_2 obtained by ALD with varying GeO_2/ZrO_2 cycle ratios: **a** Zr 3d, **b** O 1 s, and **c** Ge 2p, **d** GeO_2 contents obtained from XPS O 1 s core level spectra and Ge mol% in Ge-doped ZrO_2 as a function of the GeO_2/ZrO_2 cycle ratio in ALD.

Table 1 Summary of the electrical properties of MOS capacitors obtained by ALD with varying GeO_2/ZrO_2 cycle ratios

ALD cycle ratio (GeO_2/ZrO_2)	Ge contents (mol%)	Dielectric constant	D_{it} (cm^{-2} eV^{-1})	Hysteresis (mV)	Leakage current at − 1 MV cm (A cm^{-2})
ZrO_2	–	16.1	1.95×10^{12}	~100	6.48×10^{-8}
1:128	0.29	18.5	1.11×10^{12}	~200	7.73×10^{-8}
1:64	0.45	18.2	6.09×10^{11}	~200	1.04×10^{-7}
1:32	0.95	18.1	1.02×10^{12}	~200	1.06×10^{-7}
1:16	2.39	17.9	7.70×10^{11}	~200	1.18×10^{-7}
1:8	4.02	14.2	1.16×10^{12}	~200	1.92×10^{-7}
1:4	9.03	12.2	1.25×10^{12}	~200	2.16×10^{-7}
1:2	14.79	10.5	1.26×10^{12}	~200	2.82×10^{-7}
GeO_2	–	4.04	1.13×10^{12}	~200	6.48×10^{-7}

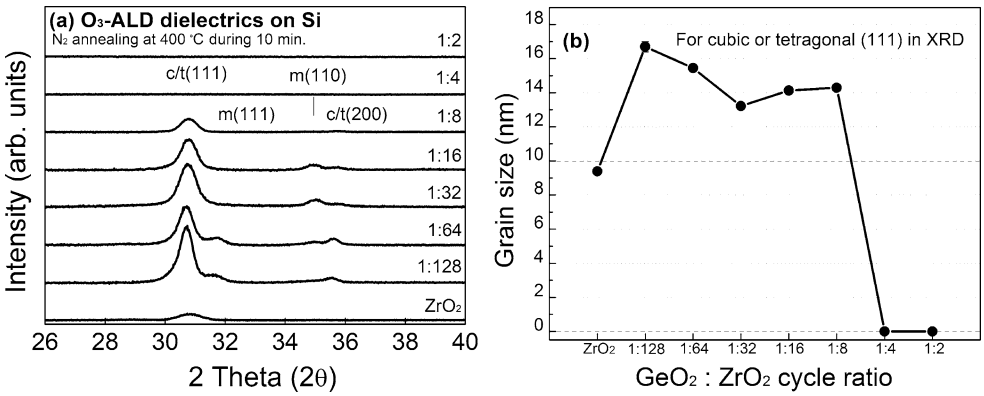

Figure 2 **a** X-ray diffraction (XRD) patterns of Ge-doped ZrO_2 films obtained by ALD with varying GeO_2/ZrO_2 cycle ratios. **b** Grain size (nm) as a function of the GeO_2/ZrO_2 cycle ratio in ALD.

thus, stabilization of cubic/tetragonal ZrO_2 does not occur significantly [26, 27]. Furthermore, the amorphous GeO_2 would be segregated, which was found in our previous study on ALD of GeO_2 with the same process conditions [28]. Therefore, increasing the ALD cycle ratio gradually decreases the intensity of cubic/tetragonal (111) peak. Furthermore, a high Ge concentration (over ~ 10%) has been known to increase the crystallization temperature of ZrO_2 to over 500 °C [29]. Corresponding to the previous results, the 1:4 and 1:2 Ge-doped ZrO_2 samples in this work showed amorphous structures with similar ranges of Ge concentration [26, 27]. Thus, we can draw the following conclusions: First, the cubic/tetragonal phase of ZrO_2 is stabilized by Ge doping. Second, the stabilization occurs for a range of Ge contents below a critical value, and the film becomes amorphous when the critical Ge content is exceeded. In addition, the cubic/tetragonal (111) diffraction peak is the prominent peak, and the grain sizes of the films were calculated using the Scherrer equation,

$$D_{\mathrm{XRD}} = K\lambda/B\cos\theta \tag{3}$$

where D, B, λ, K, and θ are the grain size, corrected full width at half maximum (FWHM), diffraction wavelength, a shape factor, and diffraction angle, respectively [30]. In Fig. 2b, the effect of Ge doping on the grain size is clearly shown, with the undoped ZrO_2 film plotted as the leftmost point. With the addition of a small amount of Ge into ZrO_2, the grain sizes significantly increased. Particularly, for the 1:128 Ge-doped ZrO_2 sample, the grain size increased from 9.39 to 16.7 nm, which is attributed to stabilization of the crystallinity of the ZrO_2 film caused by Ge doping, as shown in Fig. 2a. As the ALD cycle ratio increases, the grain size remains nearly constant until the 1:8 Ge-doped ZrO_2 sample. Further increase in Ge increased the amorphous content in the 1:4 and 1:2 Ge-doped ZrO_2 samples due to the increased crystallization temperature.

To examine the effect of Ge doping in ZrO_2 on the electrical properties of the films, MOS capacitors consisting of a Ru/17-nm-thick undoped ZrO_2, Ge-doped ZrO_2, and GeO_2/*p*-type Si structure were prepared. The C–V and I–V curves of the MOS capacitors for various GeO_2/ZrO_2 ALD cycle ratios are shown in Fig. 3a, b, respectively, and the characteristic values calculated from these graphs are summarized in Table 1. As shown in Fig. 3a, the accumulation capacitance increased with the change in the cycle ratio from 1:128 to 1:16. The accumulation capacitance is determined by $C_{\mathrm{acc}} = C_{\mathrm{ox}} = k\varepsilon_0/t$, where C_{acc}, C_{ox}, k, ε_0, and t are the accumulation capacitance, oxide capacitance, dielectric constant, permittivity of free space, and oxide thickness, respectively [31]. Since the total thickness of the dielectric was the same for all samples, the change in the accumulation capacitance is attributed to the dielectric constant. While the dielectric constant of undoped ZrO_2 is ~ 16.1, the maximum dielectric constant of Ge-doped ZrO_2 is ~ 18.5 at the ALD cycle ratio of 1:128. Modulation of the dielectric constant by doping can be attributed to the change of the crystal structure and inherent dielectric properties of the dopants. In this work, introduction of the optimal amount of Ge enhanced the crystallinity and grain size of cubic/tetragonal ZrO_2 by substituting Zr atoms with Ge atoms, which is direct evidence of the stabilization of ZrO_2 films by Ge doping. Stabilization of the cubic/tetragonal phase increases the dielectric constant by changing the unit cell volume and polarizability [32, 33]. However, introducing Ge atoms beyond the solubility limit of 3–5%, as in the 1:8 Ge-doped ZrO_2 samples in this work, will not result in significant further substitutions of Zr atoms and thus will not result in further stabilization of the cubic/tetragonal phase of ZrO_2 observed using XRD. On the contrary, segregation of amorphous GeO_2 decreases the dielectric constant due to the inherently low dielectric constant (k ~ 5–6) of GeO_2 [28]. Furthermore, amorphization of the ZrO_2 films in the 1:4 and 1:2 Ge-doped ZrO_2 also decreased the dielectric constant. Therefore, the decrease in the dielectric constants of the 1:8, 1:4, and 1:2 Ge-doped ZrO_2 relative to undoped ZrO_2 was attributed to low stabilization of the cubic/tetragonal phase of ZrO_2. The hysteresis related to the trapped oxide charges and the D_{it} values do not significantly change with Ge doping of ZrO_2, as shown in Table 1. Thus, we observed that Ge doping of ZrO_2 does not significantly change the bulk and interface qualities and is achieved without significant degradation of the film.

Figure 3b shows the insulating properties of the Ge-doped ZrO_2 films as a function of the ALD cycle ratio. The leakage current density is observed at -1 MV cm^{-1} in the I–V measurements. With an increase in GeO_2 cycle ratio, the leakage current density at -1 MV cm^{-1} (shown in Table 1) increased gradually. The leakage current density in gate dielectrics can be affected by various factors,

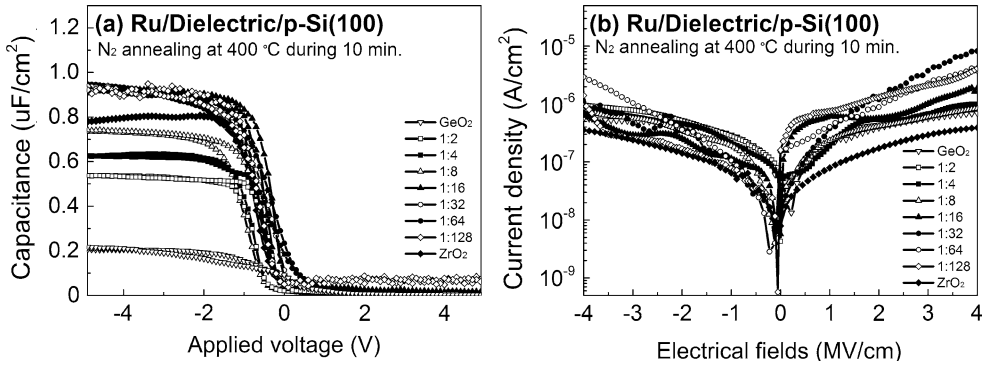

Figure 3 Electrical characteristic of MOS capacitors based on 17-nm-thick Ge-doped ZrO_2 films obtained by ALD with varying GeO_2/ZrO_2 cycle ratio: **a** C–V curves and **b** I–V curves.

such as band structure, trapped charge, film morphology. The energy bandgap of dielectrics is a key factor for the leakage current since it acts as an energy barrier against field-assisted thermionic emission of electrons by the Schottky effect [34]. However, ZrO_2 and GeO_2 have similar bandgap ranges (~ 5–6 eV) [35]; thus, a significant change in bandgap energy by Ge doping into ZrO_2 is not expected. Also, the values of bandgap energies are large enough to block the Schottky emission of electrons. The trapped charges inside the bandgap can increase the leakage current by Pool–Frenkel emission and trap-assisted tunneling [34, 36]. The trapped charge densities can be estimated from the C–V curves, as shown in Table 1, but the hysteresis related to the trapped oxide charges and the interface trap density (D_{it}) values do not significantly change with Ge doping of ZrO_2. Meanwhile, the crystal structures are affected by Ge concentration, as shown in Fig. 2. Although 1:128 Ge-doped ZrO_2 has the maximum grain size, a further increase in Ge concentration reduces the grain size of ZrO_2, which leads to an increase in the volume density of the grain boundary in the films [37]. The grain boundary has been considered as a critical leakage path in gate dielectrics [38–40]. Along the grain boundary, surface depressions form and reduce the thickness of the films at the grain boundary relative to the area inside the grains [38]. Thus, since the electric field across the film is concentrated at a relatively thin spot, the leakage current increases due to significant electron emission [39]. Moreover, since the grain boundary is an unstable region compared to the grain, impurities such as oxygen vacancies in metal oxides have a stable energy state at the grain boundary [38]. The segregated impurities at the grain boundary present favorable percolation paths for electron tunneling through the film, leading to a high leakage current [38]. Therefore, we conclude that the increase in the number of grain boundaries would be predominantly responsible for the high leakage current density with increasing Ge concentration.

The change in the dielectric constant (k) and leakage current density depending on the ALD cycle ratio is shown in Fig. 4. With increasing ALD cycle ratio, the dielectric constant improved from 16.1 to 18.5 due to the stabilization of the cubic/tetragonal phase of ZrO_2. For higher Ge contents, it rapidly decreased because of the crystallization of low-k GeO_2 and amorphization of the film. However, the leakage current density gradually increased from 6.48×10^{-8} A cm^{-2} (undoped ZrO_2) to 2.82×10^{-7} A cm^{-2} (1:2 Ge-doped ZrO_2). This is attributed to the increase in the number of grain boundary caused by the reduction in the grain size.

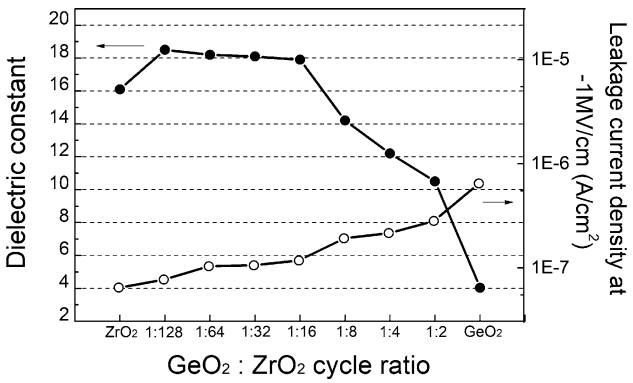

Figure 4 Dielectric constant (closed circle) and leakage current density (open circle) of Ge-doped ZrO_2 obtained by ALD as a function of the GeO_2/ZrO_2 cycle ratio.

Conclusion

In summary, we investigated the chemical, crystallographic, and dielectric properties of undoped ZrO_2 and Ge-doped ZrO_2 films deposited by ALD on p-type Si substrates. Using $Ge(O^nBu)_4$ and (C_5H_5)-$Zr[N(CH_3)_2]_3$ as precursors, stoichiometric films were obtained with negligible impurities. An ALD supercycle, which offers easy control over the dopant contents, was utilized to achieve various Ge contents ranging from 0.29 to 14.79 mol% by controlling the ALD cycle ratio (GeO_2/ZrO_2). We systematically demonstrated that the electrical properties including the dielectric constant, interface trap density, hysteresis, and leakage current density vary according to the crystallographic properties of the Ge-doped ZrO_2 films, based on XRD studies. We confirmed that the cubic/tetragonal phases of Ge-doped ZrO_2 films were stabilized due to Ge incorporation into ZrO_2. By varying the ALD cycle ratio, the dielectric properties of Ge-doped ZrO_2 can be improved and optimized for use in future nanoscale devices.

Acknowledgements

This work was partly supported by the Materials and Components Technology Development Program of MOTIE/KEIT [10080642, Development on precursors for carbon/halogen-free thin film and their delivery system for high-*k*/metal gate application] and (in part) by the Yonsei University Research Fund (Post Doc. Researcher Supporting Program) of 2017 (Project No.: 2017-12-018). This work was also supported by Air Liquide as a precursor supplier.

Authors' contribution

The manuscript was written through contributions of all authors. All authors have given approval of the final version of the manuscript.

Electronic supplementary material: The online version of this article (https://doi.org/10.1007/s10853-018-2695-4) contains supplementary material, which is available to authorized users.

References

[1] Botzakaki MA, Xanthopoulos N, Makarona E, Tsamis C, Kennou S, Ladas S, Georga SN, Krontiras CA (2013) Microelectronic Engineering ALD deposited ZrO_2 ultrathin layers on Si and Ge substrates : a multiple technique characterization. Microelectron Eng 112:208–212

[2] Robertson J (2008) Maximizing performance for higher K gate dielectrics. J Appl Phys 104(12):1–7

[3] Wallace RM, Wilk GD (2003) High-κ dielectric materials for microelectronics. Crit Rev Solid State Mater Sci 28(4):231–285

[4] Zhao X, Vanderbilt D (2002) First-principles study of structural, vibrational, and lattice dielectric properties of hafnium oxide. Phys Rev B 65(23):75105

[5] Park B-E, Oh I-K, Mahata C, Lee CW, Thompson D, Lee HBR, Maeng WJ, Kim H (2017) Atomic layer deposition of Y-stabilized ZrO2 for advanced DRAM capacitors. J Alloys Compd 722:307–312

[6] Goff J, Hayes W, Hull S, Hutchings M, Clausen K (1999) Defect structure of yttria-stabilized zirconia and its influence on the ionic conductivity at elevated temperatures. Phys Rev B 59(22):14202–14219

[7] Sasaki K, Hasu T, Sasaki K, Hata T (2002) Limited reaction growth of YSZ (ZrO_2: Y_2O_3) thin films for gate insulator. Vacuum 66:403–408

[8] Zhao CZ, Taylor S, Werner M, Chalker PR, Murray RT, Gaskell JM, Jones AC (2009) Dielectric relaxation of lanthanum doped zirconium oxide. J Appl Phys 105(4):44102

[9] Jõgi I, Kukli K, Ritala M, Leskelä M, Aarik J, Aidla A, Lu J (2010) Atomic layer deposition of high capacitance density Ta_2O_5–ZrO_2 based dielectrics for metal-insulator-metal structures. Microelectron Eng 87:144–149

[10] Li P, Chen I-W, Penner-Hahn JE (1994) Effect of dopants on zirconia stabilization—an X-ray absorption study: I, Trivalent Dopants. J Am Ceram Soc 77(5):1289–1295

[11] Lee MS, An C-H, Lim JH, Joo J-H, Lee H-J, Kim H (2010) Characteristics of Ce-doped ZrO_2 dielectric films prepared by a solution deposition process. J Electrochem Soc 157(6):G142–G146

[12] Tomida K, Kita K, Toriumi A, Tomida K, Kita K, Toriumi A (2016) Dielectric constant enhancement due to Si incorporation into HfO_2. Appl Phys Lett 89:142902

[13] Fischer D, Kersch A (2008) The effect of dopants on the dielectric constant of HfO[sub 2] and ZrO[sub 2] from first principles. Appl Phys Lett 92:12908

[14] Tsoutsou D, Apostolopoulos G, Galata SF, Tsipas P, Sotiropoulos A, Mavrou G, Panayiotatos Y, Lagoyannis A, Karydas AG, Kantarelou V, Harissopoulos S, Tsoutsou D, Apostolopoulos G, Galata SF, Tsipas P, Sotiropoulos A

(2009) Stabilization of very high- k tetragonal phase in Ge-doped ZrO_2 films grown by atomic oxygen beam deposition Stabilization of very high- k tetragonal phase in Ge-doped ZrO_2 films grown by atomic oxygen beam deposition. J Appl Phys 106:24107

[15] Tsoutsou D, Apostolopoulos G, Galata S, Tsipas P, Sotiropoulos A, Mavrou G, Panayiotatos Y (2009) Microelectronic Engineering Stabilization of a very high- k tetragonal ZrO_2 phase by direct doping with germanium. Microelectron Eng 86:1626–1628

[16] Kim H, Lee HBR, Maeng WJ (2009) Applications of atomic layer deposition to nanofabrication and emerging nanodevices. Thin Solid Films 517(8):2563–2580

[17] Zang Z, Nakamura A, Temmyo J (2013) Single cuprous oxide films synthesized by radical oxidation at low temperature for PV application. Opt Express 21(9):11448–11456

[18] Izaki M, Shinagawa T, Mizuno KT, Ida Y, Inaba M, Tasaka A (2007) Electrochemically constructed p-Cu_2O/n-ZnO heterojunction diode for photovoltaic device. J Phys D Appl Phys 40(11):3326–3329

[19] Oh I-K, Kim K, Lee Z, Song J-G, Lee CW, Thompson D, Lee H-B-R, Kim W-H, Maeng WJ, Kim H (2015) In situ surface cleaning on a Ge substrate using TMA and $MgCp_2$ for HfO_2 -based gate oxides. J Mater Chem C 3(19):4852–4858

[20] Zhitomirsky VN, Kim SK, Burstein L, Boxman RL (2010) X-ray photoelectron spectroscopy of nano-multilayered Zr-O/Al-O coatings deposited by cathodic vacuum arc plasma. Appl Surf Sci 256(21):6246–6253

[21] Mi Y, Wang J, Yang Z, Wang Z, Wang H, Yang S (2014) A simple one-step solution deposition process for constructing high-performance amorphous zirconium oxide thin film. RSC Adv 4(12):6060–6067

[22] Kibel MH (1996) X-ray photoelectron spectroscopy study of optical waveguide glasses. Surf Interface Anal 24(9):605–610

[23] Natsume Y, Sakata H (2000) Zinc oxide films prepared by sol-gel spin-coating. Thin Solid Films 372:30–36

[24] Yousfi EB, Weinberger B, Donsanti F, Cowache P, Lincot DU (2001) Atomic layer deposition of zinc oxide and indium sulfide layers for Cu (In, Ga)Se_2 thin-film solar cells. Thin Solid Films 387(1–2):29–32

[25] Lamperti L, Lamagna G, Congedo S Spiga (2011) Cubic/tetragonal phase stabilization in high-κ ZrO_2 thin films grown using O_3-based atomic layer deposition. J Electrochem Soc 158(10):G221–G226

[26] Utkin AV, Bulina NV, Belen IV, Baklanova NI (2012) Phase analysis of the ZrO_2–GeO_2 system. Inorg Chem 48(6):601–606

[27] Kim D-J, Jang J-W, Jung H-J, Huh J-W, Yang I-S (1995) Determination of solid solubility limit of GeO_2 in 2 mol Y203-stabilized tetragonal ZrO_2 by Raman spectroscopy. J Mater Sci Lett 14(14):1007–1009

[28] Yoon CM, Oh I-K, Lee Y, Song J-G, Lee SJ, Myoung J-M, Kim HG, Moon H-S, Shong B, Lee H-B-R, Kim H (2018) Water-erasable memory device for security applications prepared by the atomic layer deposition of GeO_2. Chem Mater 30(3):830–840

[29] Borilo LP, Borilo LN (2011) Physicochemical processes involved in synthesis of thin films based on double oxides of the ZrO_2-GeO_2 system. Russ J Inorg Chem 56(6):835–840

[30] Monshi A (2012) Modified Scherrer equation to estimate more accurately nano-crystallite size using XRD. World J Nano Sci Eng 2(3):154–160

[31] Robertson J (2004) High dielectric constant oxides. Eur Phys J Appl Phys 28:265–291

[32] Thompson DP, Dickins AM, Thorp JS (1992) The dielectric properties of zirconia. J Mater Sci 27:2267–227110.1007/BF01117947

[33] Toriumi A, Kita K, Tomida K, Yamamoto Y (2006) Doped HfO_2 for higher-k dielectrics. ECS Trans 1(5):185–197

[34] Cheong KY, Moon JH, Kim HJ, Bahng W, Kim NK (2008) Current conduction mechanisms in atomic-layer-deposited HfO_2 /nitrided SiO_2 stacked gate on 4H silicon carbide. J Appl Phys 103(8):1–8

[35] Cox SFJ, Gavartin JL, Lord JS, Cottrell SP, Gil JM, Alberto HV, Piroto Duarte J, Vilão RC, Ayres De Campos N, Keeble DJ, Davis EA, Charlton M, Van Der Werf DP (2006) Oxide muonics: II. Modelling the electrical activity of hydrogen in wide-gap and high-permittivity dielectrics. J Phys: Condens Matter 18(3):1079–1119

[36] Yu SM, Guan XM, Wong HSP (2011) Conduction mechanism of TiN/HfOx/Pt resistive switching memory: a trap-assisted-tunneling model. Appl Phys Lett 99(6):63507

[37] Kim H, Yang S, Park K (2013) Leakage current analysis depends on grain size variation in zinc oxide thin film transistor. 224th ECS Meeting. https://ecs.confex.com/ecs/224/webprogram/Abstract/Paper23102/A1-0076.pdf

[38] McKenna K, Shluger A, Iglesias V, Porti M, Nafría M, Lanza M, Bersuker G (2011) Grain boundary mediated leakage current in polycrystalline HfO_2 films. Microelectron Eng 88(7):1272–1275

[39] Park BE, Oh IK, Lee CW, Lee G, Shin YH, Lansalot-Matras C, Noh W, Kim H, Lee HBR (2016) Effects of Cl-based ligand structures on atomic layer deposited HfO_2. J Phys Chem C 120(11):5958–5967

[40] Bersuker G, Yum J, Vandelli L, Padovani A, Larcher L, Iglesias V, Porti M, Nafría M, McKenna K, Shluger A, Kirsch P, Jammy R (2011) Grain boundary-driven leakage path formation in HfO_2 dielectrics. Solid State Electron 65–66(1):146–150